IOWA STATE UNIVERSITY
Digital Repository

Materials Science and Engineering Publications | Materials Science and Engineering

5-2004

Microscopic Observations of Voids in Anodic Oxide Films on Aluminum

R. Huang
Iowa State University

Kurt R. Hebert
Iowa State Univ,, krhebert@iastate.edu

L. Scott Chumbley
Iowa State University, chumbley@iastate.edu

Follow this and additional works at: http://lib.dr.iastate.edu/mse_pubs

Part of the Metallurgy Commons

The complete bibliographic information for this item can be found at http://lib.dr.iastate.edu/mse_pubs/149. For information on how to cite this item, please visit http://lib.dr.iastate.edu/howtocite.html.

This Article is brought to you for free and open access by the Materials Science and Engineering at Iowa State University Digital Repository. It has been accepted for inclusion in Materials Science and Engineering Publications by an authorized administrator of Iowa State University Digital Repository. For more information, please contact digirep@iastate.edu.

Microscopic Observations of Voids in Anodic Oxide Films on Aluminum

Abstract
The relationship was explored between nanoscale voids in anodic aluminum oxide films and the surface condition of aluminum samples prior to anodizing. Transmission electron microscopy (TEM) detected voids on the order of 10 nm in anodic films. Atomic force microscopy (AFM) of these films, obtained after partial oxide dissolution, revealed surface cavities; comparison of TEM and AFM suggested that the cavities were the oxide voids. AFM images after variable extents of oxide dissolution showed that the voids were distributed evenly through the inner 60% of the film thickness, indicating that they were formed at the metal-oxide interface during film growth. Both AFM and TEM showed that the void concentration in the film was sensitive to the extent of dissolution of the aluminum samples in NaOH prior to anodizing. Positron annihilation spectroscopy had previously detected voids in samples without anodic films, located in the metal near the oxide-metal interface; the quantity of these interfacial voids was controlled by NaOH dissolution. The void concentration in the inner part of the anodic films was proportional to the quantity of these pre-existing interfacial voids. It was inferred that the oxide voids were formed by incorporation, during anodizing, of interfacial metal voids into the oxide film. The uniform concentration of oxide voids in the inner film suggested that interfacial metal voids formed continuously during anodizing and that metal voids were generated repeatedly at specific interfacial sites during film growth.

Keywords
Ames Laboratory, Chemical Engineering

Disciplines
Metallurgy

Comments
This article is from Journal of The Electrochemical Society 151 (2004): 379-386, doi: 10.1149/1.1753582.

This article is available at Iowa State University Digital Repository: http://lib.dr.iastate.edu/mse_pubs/149

Journal of The Electrochemical Society, **151** (7) B379-B386 (2004)
0013-4651/2004/151(7)/B379/8/$7.00 © The Electrochemical Society, Inc.

Microscopic Observations of Voids in Anodic Oxide Films on Aluminum

R. Huang,[a,*] K. R. Hebert,[a,,z] and L. S. Chumbley[b]**

[a]*Department of Chemical Engineering and* [b]*Ames Laboratory-U.S. Department of Energy, and Department of Materials Science and Engineering, Iowa State University, Ames, Iowa 50011, USA*

The relationship was explored between nanoscale voids in anodic aluminum oxide films and the surface condition of aluminum samples prior to anodizing. Transmission electron microscopy (TEM) detected voids on the order of 10 nm in anodic films. Atomic force microscopy (AFM) of these films, obtained after partial oxide dissolution, revealed surface cavities; comparison of TEM and AFM suggested that the cavities were the oxide voids. AFM images after variable extents of oxide dissolution showed that the voids were distributed evenly through the inner 60% of the film thickness, indicating that they were formed at the metal-oxide interface during film growth. Both AFM and TEM showed that the void concentration in the film was sensitive to the extent of dissolution of the aluminum samples in NaOH prior to anodizing. Positron annihilation spectroscopy had previously detected voids in samples without anodic films, located in the metal near the oxide-metal interface; the quantity of these interfacial voids was controlled by NaOH dissolution. The void concentration in the inner part of the anodic films was proportional to the quantity of these pre-existing interfacial voids. It was inferred that the oxide voids were formed by incorporation, during anodizing, of interfacial metal voids into the oxide film. The uniform concentration of oxide voids in the inner film suggested that interfacial metal voids formed continuously during anodizing and that metal voids were generated repeatedly at specific interfacial sites during film growth.
© 2004 The Electrochemical Society. [DOI: 10.1149/1.1753582] All rights reserved.

Manuscript submitted March 28, 2003; revised manuscript received January 25, 2004. Available electronically May 19, 2004.

Various surface defects have been proposed to act as sites for corrosion pit initiation on pure metals, including dislocations, microsegregated impurities, and flaws in the surface oxide film.[1] However, as yet there is no general agreement on the nature of pit precursor sites. Recently, positron annihilation spectroscopy (PAS) has been used to detect nanometer-scale voids in aluminum metal, located within 100 nm of the metal-oxide film interface.[2-4] The measurements indicated that the void surfaces were free of oxide, suggesting a high reactivity if exposed during uniform corrosion. Therefore, the possibility that the interfacial voids act as initiation sites for pitting corrosion was explored. Atomic force microscopy (AFM), after chemical stripping of the oxide film in CrO_3-H_3PO_4 solution, revealed surface cavities, the depth and area coverage of which agreed with PAS measurements of buried voids. Further, the sites of these cavities corresponded to those of corrosion pits, suggesting that the voids may act as pit precursor sites.[3,4] Surface treatments such as NaOH dissolution, which are used in etching applications to enhance the pit number density, also generated increased numbers of voids.[3] The void number density estimated from AFM was comparable to that of pits formed during anodic etching.[4]

Because PAS indicated that the voids are at least of nanometer size, an attempt was made here to view them by high-resolution microscopic techniques. The visualization of voids can yield information not obtainable with PAS about their size, morphology, and location relative to surface features such as chemical or structural inhomogeneities. Direct observations of interfacial voids in the metal using cross-sectional TEM may be possible.[5] However, given the typical number densities of pitting sites, the relatively small interface area sampled by these cross sections may not permit pit precursor defects such as voids to be effectively viewed. However, one can expect the interfacial voids in the metal to be incorporated into the oxide during anodic film growth as the metal layer containing voids is oxidized. Assuming that the volume change accompanying incorporation is minor, inferences about void geometry and location would be possible from the microscopic observations of oxide voids. Plan-view microscopic images of oxide films sample a larger interface area compared to cross-sectional images, increasing the probability of finding voids. Nanoscale voids formed during anodic alumina formation have been found in prior transmission electron microscopy (TEM) studies, but were thought to derive from gas evolution.[6,7] In another study, TEM-detected voids were due to local densification during oxide crystallization after anodizing.[8]

In this work, microscopic observations of voids in anodic oxide films were carried out using both TEM and AFM. The experimental protocol is illustrated in Fig. 1. Aluminum foil samples were used in either the as-received condition or after various times of NaOH immersion at open circuit. The different samples contained variable quantities of interfacial voids in the metal, as determined by the NaOH treatment time.[3] Because anodic oxide growth occurs at both metal-oxide and oxide-solution interfaces,[9] the interfacial voids should be incorporated into the interior of the film, as shown. In some experiments, the metal underlying the anodic film was dissolved, and the remaining oxide was examined in plan view with TEM. Otherwise, the anodic film was partially dissolved in a hot acidic solution and its surface viewed with AFM; the uniformity of oxide dissolution by such procedures was established earlier.[10] As illustrated in Fig. 1, an appropriate depth of dissolution would expose the voids as surface cavities. AFM images obtained after different extents of oxide dissolution provided an assessment of the void concentration as a function of depth. This quantitative information complemented the nondestructive through-thickness TEM images.

Recently, a PAS study of anodic oxidation demonstrated that new interfacial voids in the metal are created during anodizing.[11] It was speculated that void formation involves the agglomeration of interfacial metal vacancies formed by oxidation. After the formation of such a void, continued anodic film growth would likely result in its incorporation into the oxide. The microscopic observations would then reveal voids occupying a range of depths, as opposed to the single layer of voids shown in Fig. 1 resulting from only preexisting interfacial voids. It is seen here that microscopic characterization of the void depth profiles in anodic films yielded insight into the process of interfacial void formation during anodic oxide growth. The void depth profiles obtained for samples with different NaOH pretreatment times suggested that voids are not formed at random locations on the metal-oxide interface but instead at certain favored sites. With regard to the possible function of voids as pitting sites, their association with other types of surface defects may be consistent with the empirically known correspondence between pits and surface impurities[12] or topographic asperities.[13-15]

* Electrochemical Society Student Member.
** Electrochemical Society Active Member.
z E-mail: krhebert@iastate.edu

Downloaded on 2014-09-11 to IP 129.186.176.188 address. Redistribution subject to ECS terms of use (see ecsdl.org/site/terms_use) unless CC License in place (see abstract).

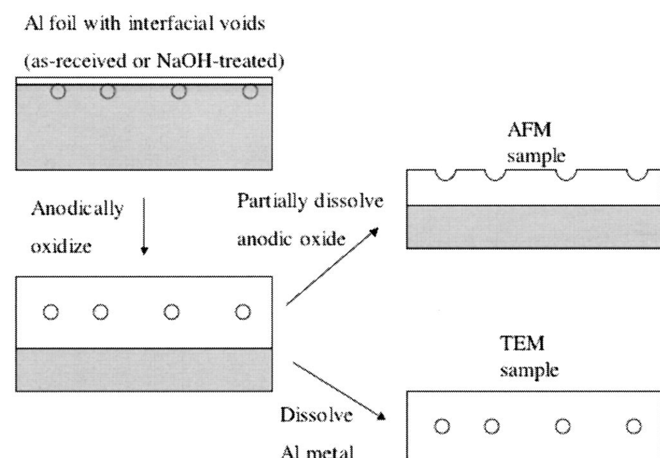

Figure 1. Schematic of the experimental protocol leading to preparation of TEM and AFM samples. Voids are represented as circles, and the metal and oxide films by shaded and white areas, respectively. The drawings illustrate the formation of oxide voids by incorporation of pre-existing interfacial voids during anodic film growth; creation of interfacial voids during anodizing and their subsequent incorporation in the film are not depicted.

Experimental

The aluminum foils used in this work were manufactured for use in aluminum electrolytic capacitors (Toyo Aluminum). The foils were 100 μm thick with a typical grain size of 100 μm, and their nominal purity was 99.98%. The large grain size is due to extensive annealing after rolling, *e.g.*, for 5-6 h at 600°C.[16] Impurities include Cr, Cu, Fe, Ga, Mg, Si, and Zn with bulk concentrations of the order 10 wt-ppm.[17]

Caustic treatment was carried out by immersion of foils in 1 N NaOH solution for different lengths of time at room temperature, after which they were washed thoroughly with deionized (DI) water. Prior to anodic oxidation, the samples were dipped in 1 N HNO_3 at ambient temperature for 1 min to avoid the erratic anodizing behavior sometimes encountered on foils anodized directly after NaOH treatment. The nitric acid dip may eliminate a gel-like surface layer formed in NaOH. For consistency, foils that had not received NaOH treatment were also dipped in nitric acid prior to anodizing. Anodic oxidation of the pretreated samples was carried out in a borate buffer solution (pH 8.5-8.7) at room temperature, at a constant applied current density of 2.5 mA/cm^2. The current source was a potentiostat/galvanostat (EG&G PAR-273), and the counter electrode was a Pt wire. Anodic oxidation continued until voltages of 27, 53, 80, and 106 V were attained *vs.* the counter electrode. After anodizing, the samples were rinsed thoroughly with DI water.

To prepare samples for TEM examination, the anodized foils were immersed in solutions of 10 vol % bromine and 90 vol % methanol until the aluminum metal was completely dissolved. The remaining oxide films were placed on copper grid holders for TEM. The films as mounted on the grids were electron transparent, so no further sample preparation was necessary. The samples were examined in a Philips CM30 scanning/transmission microscope operated at various voltages from 100 to 300 keV.

For AFM imaging, the anodized foils were cut into small pieces, on which the surface oxide films were partially stripped by immersion for different times up to 4 min in 5% H_3PO_4 at 80°C. The stripped samples were washed in DI water and dried in air before AFM imaging. To quantitatively determine the rate of film dissolution during stripping, the partly stripped foils were reanodized in borate buffer, during which the potential transients were recorded. As discussed in the results and discussion section, the fraction of the oxide thickness removed during stripping could be inferred from these potential transients. AFM imaging was carried out in direct contact mode, using a 14 μm scanner with Si cantilevers and a Si_3N_4 tip (Digital Instruments Nanoscope III). The photodiode voltage was set to 4.60 V; assuming a cantilever spring constant of 0.06 N/m, the estimated applied force is 1.5 nN. Each sample was imaged four to five times at different positions, using a typical scan area of 5 × 5 μm. The top view images presented here were further magnified by cropping and enlarging, and a "sharpen filter" (Adobe Photoshop) was used to highlight the small features of interest.

Results and Discussion

TEM.—During anodizing both NaOH-treated and untreated foils, the potential increased at a constant rate of 1.1 ± 0.05 V/s. From Faraday's law and the forming voltage-thickness ratio of 1.3-1.4 nm/V,[18] a 100% current efficiency for oxide growth would imply a rate of potential increase of 1.15 V/s at 2.5 mA/cm^2. Hence, the potential-time slopes indicate current efficiencies of approximately 100%.

TEM images of 106 V anodic films after dissolution of the aluminum substrate are presented in Fig. 2 and 3. The film in Fig. 2 was formed on a foil that had been treated in NaOH for 5 min, whereas that in Fig. 3 had received no NaOH treatment. Selected area electron diffraction confirmed that the anodic films in both cases were amorphous. White features, many of which are roughly circular, are apparent at higher magnification. Examples of these features are

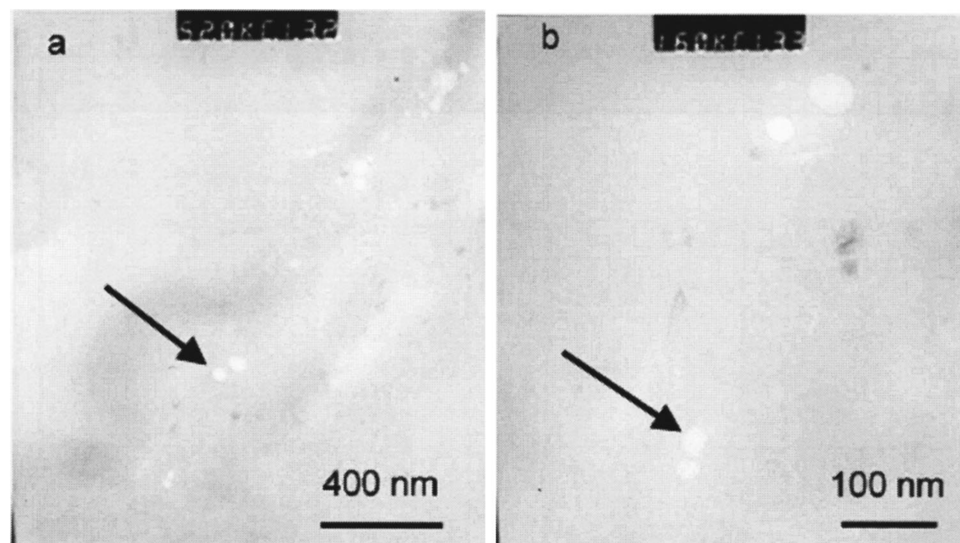

Figure 2. TEM images of anodic aluminum oxide film formed to 106 V on aluminum foil treated in NaOH for 5 min. (a) Low magnification and (b) high magnification.

Downloaded on 2014-09-11 to IP 129.186.176.188 address. Redistribution subject to ECS terms of use (see ecsdl.org/site/terms_use) unless CC License in place (see abstract).

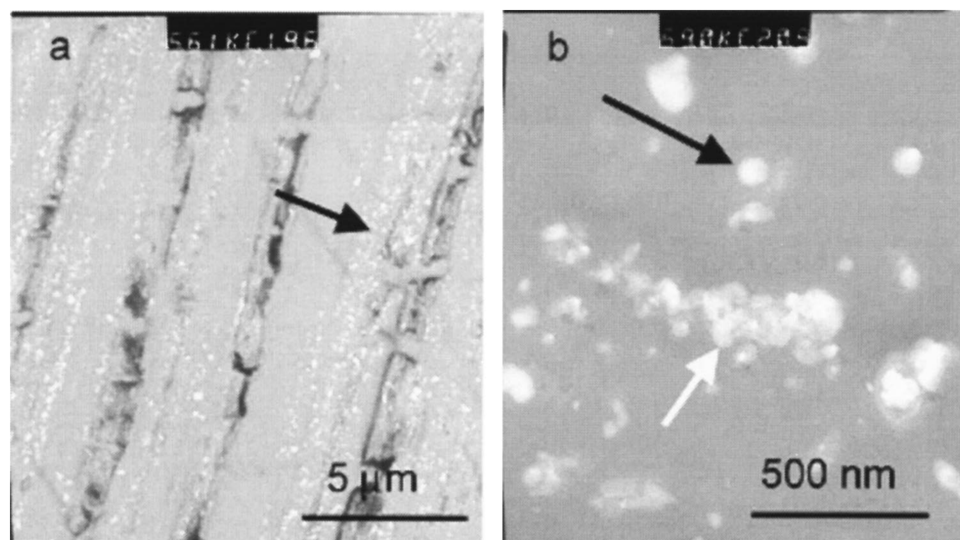

Figure 3. TEM images of anodic aluminum oxide film formed to 106 V on aluminum foil with no NaOH treatment. (a) Low magnification and (b) high magnification.

indicated by arrows in Fig. 2a,b and Fig. 3b. No diffraction could be obtained from these features, or from the surrounding material. Stereopair imaging was carried out and confirmed that the circular features in Fig. 2 are voids within the film. However, some white features in the as-received sample were found to be voids contained in the film (*e.g.*, indicated by the black arrow in Fig. 3b), and others are pores through the film thickness (*e.g.*, indicated by the white arrow in Fig. 3b).

Clear differences in void size and distribution are apparent between Fig. 2 and 3. The voids in Fig. 2 appeared scattered throughout the sample. Because of their small size and low associated contrast, they were not detected except at high magnification, and their number density could not be estimated reliably. Linear strings of voids were often seen, indicating that some common feature has determined their position. For example, in Fig. 2a, the voids are distributed along a slightly thicker region of the film implied by the band of darker contrast running from the upper right corner to the lower left. Such regions of thicker film may have been found along the ubiquitous surface ridges apparent in AFM images, as discussed later. In a sample of 18 voids, the diameter was distributed about a mean of 42 nm with a standard deviation of 13 nm; the largest and smallest voids were 67 and 25 nm diam.

In contrast to Fig. 2, voids and pores in the film on the as-received foil were readily visible at relatively low magnification. Figure 3a is representative of a randomly chosen area of this size. Bands of voids and pores, such as that indicated by the arrow, run along bands of thicker film. These bands are roughly parallel to one another and correspond to rolling lines on the foil surface. Preferential etch pit formation along rolling lines on as-annealed foils has been noted earlier, suggesting that pit precursor defects are located there.[15,19] From a sample of 36 voids and pores, the average diam was 76 nm with a standard deviation of 52 nm; the largest and smallest diam were 208 and 22 nm. From the clear differences of size, appearance, and distribution of voids in films on treated and untreated samples, void formation during anodizing is clearly sensitive to the foil's pre-existing surface condition.

Chemical stripping of the anodic oxide film.—To detect the oxide voids with AFM, the anodic films were partly dissolved in a phosphoric acid stripping bath, and then their surfaces were imaged. Knowledge of the rate and uniformity of oxide dissolution during stripping was required to interpret the AFM images in terms of the depth distribution of voids in the film. This information was obtained from potential measurements during constant current reanodizing of the samples with partially dissolved oxide films. The oxide film thickness after stripping is revealed by these measurements, as it is related to the measured anodizing voltage by a constant factor of 1.3-1.4 nm/V.[18] Takahashi *et al.* confirmed this relationship between the reanodizing potential and film thickness, using film thickness from capacitance measurements and TEM, as well as obtaining the mass of oxide dissolved from chemical analysis of the stripping solution.[10]

Potential-time curves during reanodizing in borate buffer solutions are shown in Fig. 4 for several samples with different NaOH treatment times. In all cases, the anodic film had been formed to 106 V and then stripped for 60 s in phosphoric acid. In each potential transient, the potential at first increased at a constant rate up to 80 V, at which point the slope abruptly decreased. The initial slope increased with NaOH treatment time, whereas the slope above 80 V was the same for all samples. The final voltage of 110 V in the figure is the voltage limit of the power supply.

Potential transients with rapid slope changes like those in Fig. 4 were observed previously during the anodic oxidation of aluminum substrates that were covered by alumina films of known porosity.[20,21] Analysis of these experiments showed that, at the outset of anodizing, the applied current flowed only to the pore bottoms, where the oxide thickness was smallest; hence, the local film growth current density was larger than the applied current density.

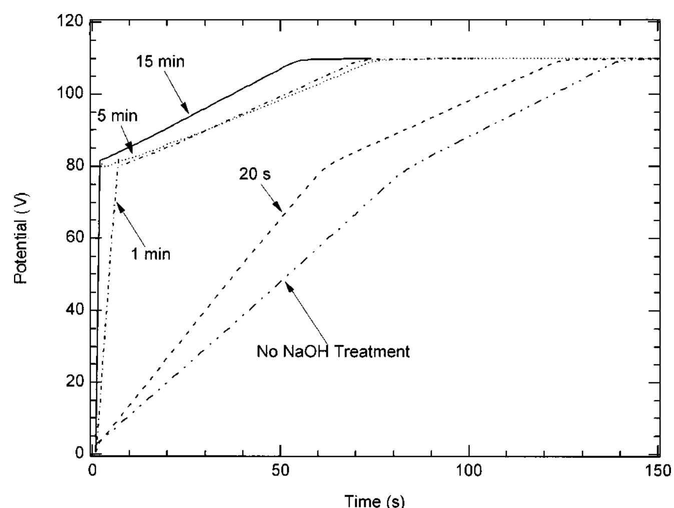

Figure 4. Potential-time curves during reanodizing aluminum after partial stripping of the anodic oxide film. Films were originally formed to 106 V and then chemically stripped for 1 min in H_3PO_4. The parameter is the NaOH treatment time prior to the first anodization.

Downloaded on 2014-09-11 to IP 129.186.176.188 address. Redistribution subject to ECS terms of use (see ecsdl.org/site/terms_use) unless CC License in place (see abstract).

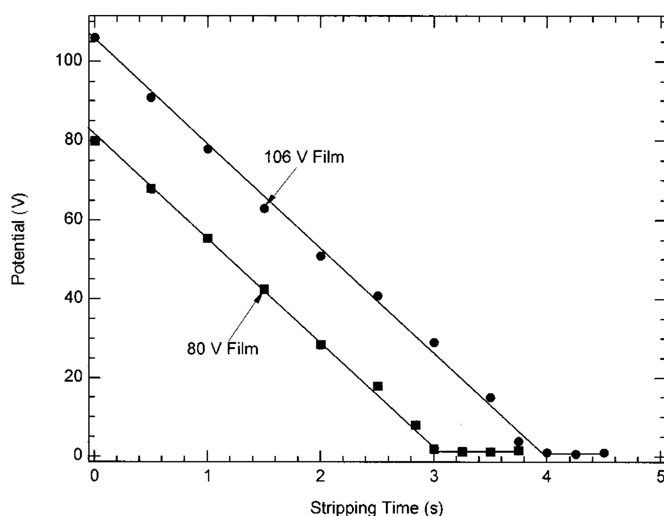

Figure 5. Potential at the slope change during reanodizing (see Fig. 4) *vs.* stripping time in H_3PO_4. Aluminum foils were treated in NaOH for 5 min, and then anodic films were formed to the indicated voltages.

This rapid film growth was associated with a high rate of potential rise, which decreased with increasing porosity. When the pores were completely filled with oxide, the slope of the potential transient decreased suddenly; at this time, the film began to grow uniformly across the surface, at a reduced rate equivalent to the applied current density.

Therefore, the abrupt slope changes in Fig. 4 indicate that the partially stripped anodic films were porous. According to this interpretation, the porosity was largest in the anodic film on the as-received foil and decreased to low values as the NaOH treatment time was increased to 5 min. This trend is consistent with the TEM observations, which revealed through-pores in the film on the as-received foil, which are likely responsible for the small potential-time slope on this sample. However, the voids in the film on the 5 min NaOH-treated sample were smaller and isolated and did not appear to form continuous pores. This relatively nonporous film morphology is consistent with the high initial potential-time slope for this sample. Finally, note that the common slope of the potential transients above 80 V is ~0.5 V/s, significantly smaller than the value of 1.1 V/s expected for 100% current efficiency. This suggests a reduced current efficiency after stripping, possibly due to a surface layer left by the phosphoric acid stripping procedure.

AFM observations were confined to foils with at least 1 min NaOH treatment, on which the film porosity was small and stripping was expected to proceed uniformly. Because the film thickness and forming voltage are proportional, the progress of stripping could be inferred from the potential at the slope change during reanodizing. For example, in Fig. 4, the fraction of the anodized film thickness that remains after stripping is (80 V)/(106 V), or 0.75. Figure 5 shows the potential at the slope change plotted as a function of stripping time. Data for two anodic film thicknesses are given, for the same NaOH treatment time of 5 min. The linear decrease of potential shows that film thinning occurred uniformly and at a constant rate. Assuming a film thickness/voltage ratio of 1.4 nm/V, the stripping rate was approximately 35 nm/min, independent of initial film thickness. The reanodizing voltage decreased linearly to ~1.5 V, after which it remained constant, indicating complete removal of the anodically formed oxide. The constant dissolution rate permitted the stripping time to be calibrated in terms of film thickness; thus, the fraction of the film thickness removed is the ratio of the stripping time to the time for complete dissolution of the anodic film.

The relatively slow, uniform oxide dissolution during stripping indicated that it could be used in conjunction with AFM surface imaging to determine the depth profiles of voids or other defects in the film. Because of the slow dissolution, enlargement of void size or distortion of shape by dissolution should be minimized. This expectation was examined further by comparison of TEM and AFM results, as described in detail in the following paragraphs.

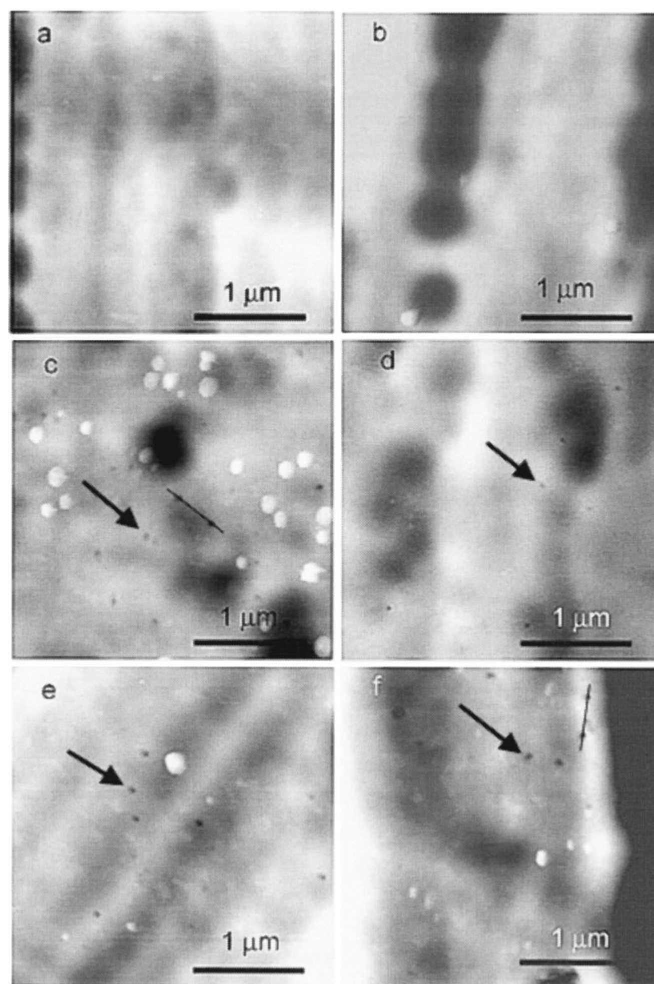

Figure 6. AFM images after partial stripping of 106 V anodic films on foils with 5 min NaOH treatment, showing effect of stripping time. Stripping times: (a) 40 s (17% of oxide film thickness removed), height contrast 128 nm; (b) 90 s (38% of oxide removed), 128 nm; (c) 120 s (50% of oxide removed), 116 nm; (d) 150 s (63% of oxide removed), 156 nm; (e) 180 s (75% of oxide removed), 156 nm; (f) 210 s (88% of oxide removed), 147 nm.

AFM observations of partially stripped anodic films.—Images of oxide film surfaces after various stages of oxide stripping are shown in Fig. 6 for a foil treated in NaOH for 5 min and then anodized to 106 V. When less than 40% of the anodic film had been dissolved, the surface morphology was unchanged by stripping (see Fig. 6a,b). However, open surface cavities with approximately circular shapes were revealed after longer stripping times (see Fig. 6c-f). The term "cavity" is applied to these pit-like features revealed by oxide stripping to distinguish them from corrosion pits. The average diam of a population of about 100 cavities was 66 nm, with a standard deviation of 18 nm. Surface height profiles are shown in Fig. 7 which correspond to the lines drawn in Fig. 6c and f; each profile spans two surface cavities. As illustrated by Fig. 7, the typical cavity depth was about 10-20 nm, suggesting a shallow, disk-like shape.

Figure 8 directly compares AFM and TEM images at the same magnification. The dark circular areas in the AFM image (cavities) correspond to the white circular spots in the TEM image (voids). Examples of both types of feature are indicated by arrows. The

Downloaded on 2014-09-11 to IP 129.186.176.188 address. Redistribution subject to ECS terms of use (see ecsdl.org/site/terms_use) unless CC License in place (see abstract).

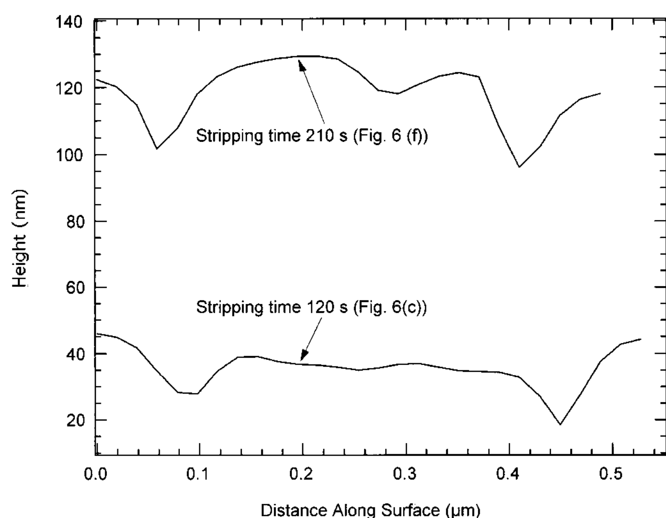

Figure 7. Surface height profiles along lines marked in Fig. 6c,f. Each scan shows the profiles of two surface cavities.

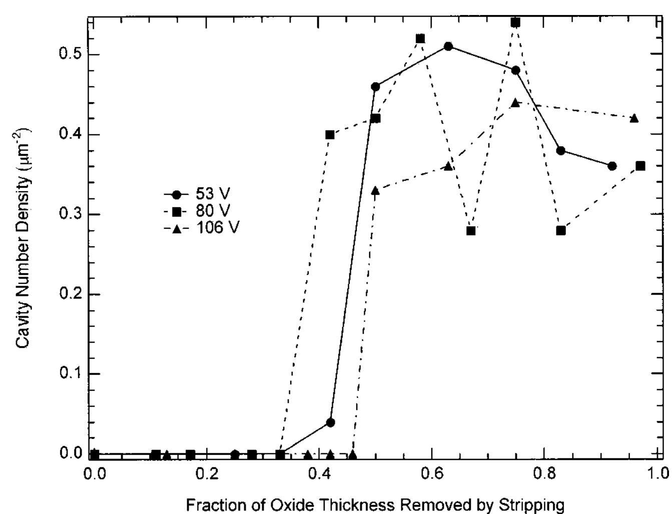

Figure 9. Cavity depth distributions in anodic films for foils with 5 min NaOH treatment. Parameter is forming voltage of anodic films.

somewhat larger average diam of the cavities (66 *vs.* 42 nm) may be the result of oxide dissolution during stripping. The increase in void radius by dissolution is roughly the product of the dissolution velocity and the time for the dissolution front to "pass" the void, *i.e.*, $V_d(H/V_d)$, where H is the void depth and V_d is the dissolution velocity. Thus, the cavity radius should be about 10 nm larger than the void radius, in good agreement with the TEM and AFM measurements. The locations of cavities and voids can also be compared. Cavities in the AFM images were preferentially distributed along ridges, which may correspond to the bands of slightly increased foil thickness associated with voids in TEM images. Considering these comparisons, one can conclude that the cavities revealed by stripping are the same as the voids in TEM images. It is not known whether the AFM and TEM images revealed all the voids in the film or only the larger voids, which represent a subset of the population.

Numerous AFM images, like those in Fig. 6, were acquired on foils treated for 5 min in NaOH for anodic forming voltages of 53, 80, and 106 V. For a given voltage, images after various stripping times were used to estimate the depth dependence of the number of voids per unit area. These estimates were based on about four images and 50 voids at each stripping time. Figure 9 presents the depth distributions as plots of void concentration *vs.* fraction of oxide film thickness removed. The plots clearly show that no voids were present in the top portion of the film, representing 40-50% of its thickness. With the thickness-voltage ratio of 1.4 nm/V, this critical fractional thickness corresponds to widely different depths of 33, 50, and 67 nm for the three films in Fig. 9. Thus, the void distribution is correlated not with depth or stripping time, but with fractional thickness.

The critical fractional thickness of 0.4-0.5 can be explained by noting that the transport number of Al^{3+} ions in the anodic film has been found to be 0.4.[22] Accordingly, 40% of the film is formed at the film-solution interface and 60% at the metal-film interface. This implies that at the outset of anodizing, the metal-film interface would have been located near the boundary between the void-containing and void-free regions in Fig. 9. During film growth, the interface swept through the range of depths corresponding to the void-containing layer in the figure. Thus, the depth profiles strongly suggest that the voids first appeared at the metal-film interface during anodic oxide growth and then remained stationary as the film increased in thickness.

Figure 9 indicates that voids are continuously distributed through the inner portion of the anodic film, with an approximately uniform concentration. This differs from the expectations based on the assumption that only pre-existing interfacial metal voids are incorpo-

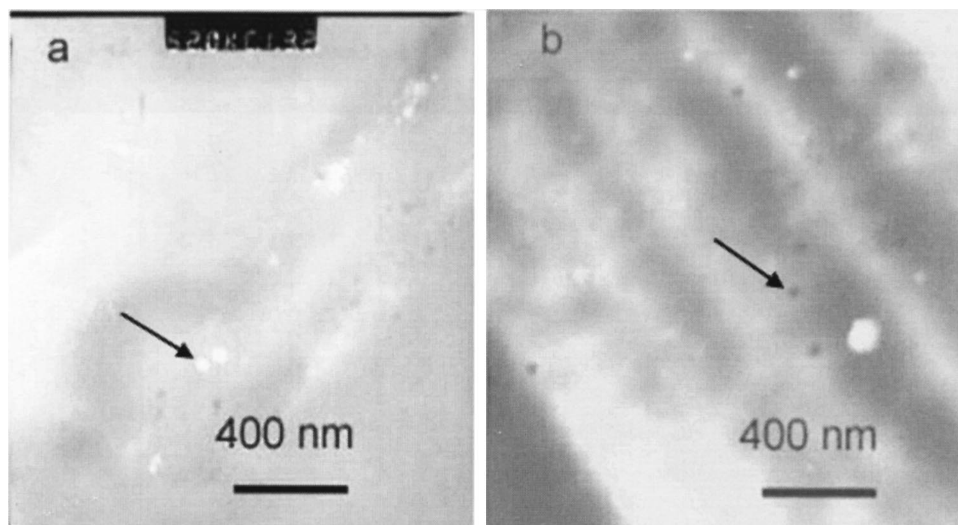

Figure 8. Comparison of TEM and AFM images of anodic aluminum oxide film formed to 106 V. Foil was treated in NaOH for 5 min before anodizing. (a) TEM and (b) AFM.

Downloaded on 2014-09-11 to IP 129.186.176.188 address. Redistribution subject to ECS terms of use (see ecsdl.org/site/terms_use) unless CC License in place (see abstract).

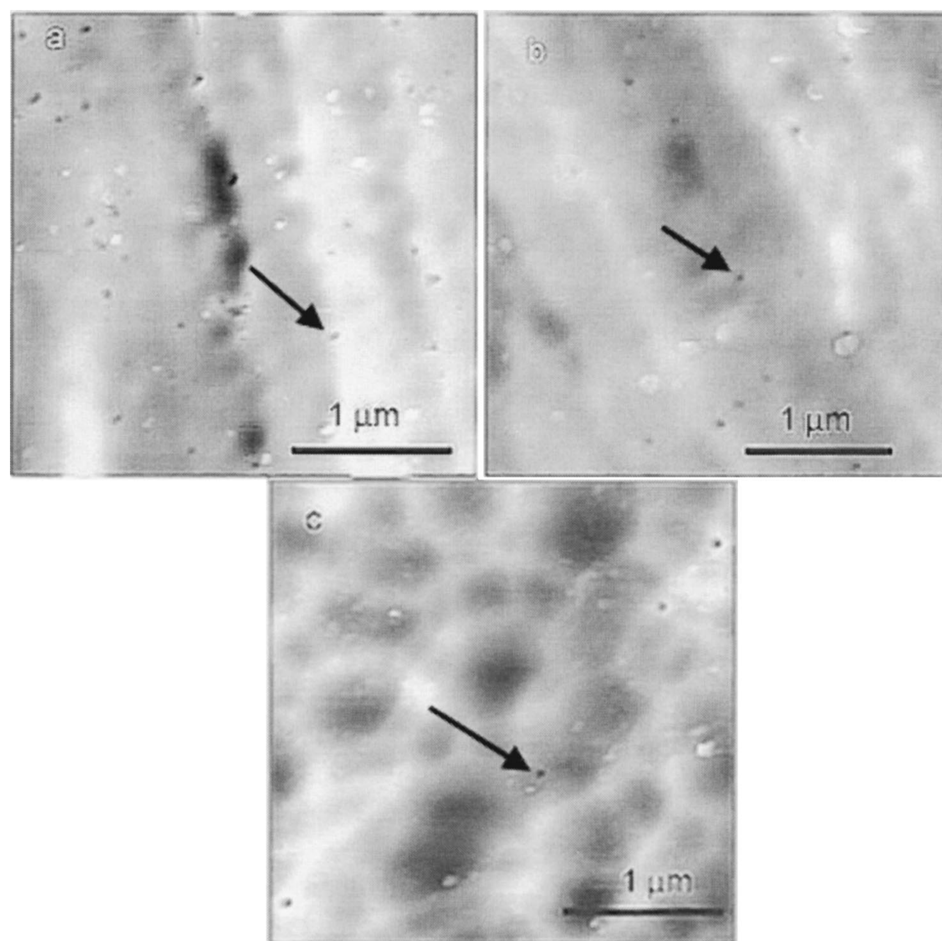

Figure 10. AFM images after partial stripping of 80 V anodic films on foils with NaOH treatment times of 1, 2, and 15 min. (a) 1 min NaOH treatment, 90 s stripping (50% of oxide film thickness removed), height contrast 158 nm. (b) 2 min NaOH treatment, 105 s stripping (58% of oxide removed), 158 nm. (c) 15 min NaOH treatment, 90 s stripping (50% of oxide removed), 77 nm.

rated in the oxide, and not interfacial voids generated during anodizing. As illustrated in Fig. 1, this assumption is consistent with a thin band of voids at a fractional depth of 0.4, having a thickness of about 30 nm, the same as the interfacial void layer detected by PAS after 5 min NaOH treatment.[3] The thickness of the void-containing layers in Fig. 8 are significantly larger (about 40, 70, and 80 nm for the three thickest films) and extend to the metal-oxide interface. These oxide voids at greater depths were likely interfacial voids in the metal which formed during anodizing and were subsequently incorporated into the film. The roughly uniform void concentrations in Fig. 9 indicate that interfacial void formation occurred at an approximately constant rate during anodizing. In the AFM images, oxide voids from pre-existing interfacial voids cannot be distinguished from those arising from interfacial voids created during anodizing.

Dependence of void distribution on NaOH pretreatment time.—AFM images of partially stripped anodic films were acquired on foils treated in NaOH for variable times up to 30 min. When the immersion was less than 1 min, large cavities were found whose depths exceeded the film thickness. These cavities were likely the result of metal dissolution at the base of the through-pores in these films detected by TEM (Fig. 3) and suggested by the reanodizing potential transients (Fig. 4). Hence, as mentioned, results are presented only for treatment times of 1 min or longer. For these NaOH immersion times, no evidence was found for metal dissolution at the base of the film.

Figure 10 shows a selection of images of partly stripped anodic films on samples with NaOH immersion times of 1, 2, and 15 min. In each case, the stripping times correspond to fractional film removals of at least 0.5, for which voids are expected, according to Fig. 9. Each image shows a large number of shallow circular voids similar to those in Fig. 6. As shown in Fig. 10a,b, foil surfaces after 1 and 2 min treatments contain parallel ridges formed during rolling, ranging from 30-200 nm in height. Most of the voids on these samples are located near the tops of the ridges. After 15 min NaOH treatment, the parallel-ridge topography has been removed by metal dissolution (dissolution rate $\sim$100 nm/min[17]), and a new surface texture formed by NaOH dissolution itself is apparent (Fig. 10c). The dissolution-generated topography is described by a mosaic pattern of scalloped depressions bordered by 10-100 nm high ridges.[17] Nearly all the voids in Fig. 10c are located at the trijunction points where three such ridges intersect. Thus, there appears to be a general tendency for voids to be located atop asperities of the metal surface topography.

Figure 11 presents void depth distributions for anodic films on a foil treated for 15 min in NaOH. As in Fig. 9, the top portion of the film is void-free. High void concentrations are found at fractional depths greater than 0.42, as is also the case in Fig. 9. A few voids are also found at depths of 0.22-0.42 in Fig. 11, which was not the case for the 5 min NaOH treatment. However, the much higher concentration at depths greater than 0.4 is again consistent with generation of voids at the metal-film interface during anodic oxide growth. The main difference between Fig. 11 and the distribution at 5 min NaOH treatment time is that a lower concentration of voids is found in the inner film. At 5 min, the void concentration in the inner film ranged from 0.3-0.5 μm^{-2}, compared to only 0.1-0.2 μm^{-2} at 15 min.

The dependence of void concentration on NaOH treatment time was explored further, using measurements over a range of NaOH treatment times. Figure 12 shows the average number density of voids in the inner film plotted *vs.* treatment time. The void concentration decreases monotonically from 1 to 30 min dissolution time. The figure also shows the defect layer S parameter (S_d) obtained by

Downloaded on 2014-09-11 to IP 129.186.176.188 address. Redistribution subject to ECS terms of use (see ecsdl.org/site/terms_use) unless CC License in place (see abstract).

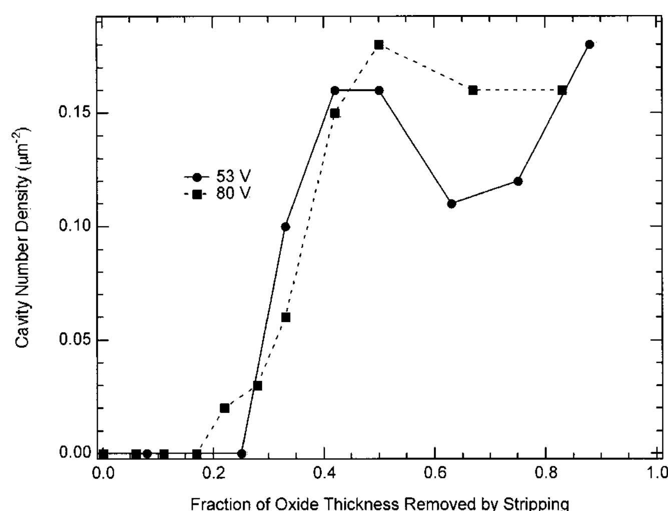

Figure 11. Cavity depth distributions in anodic films for foils with 15 min NaOH treatment. Parameter is forming voltage of anodic films.

PAS for foils that had the same NaOH treatments but had not been anodically oxidized.[3] S_d correlates with the void volume fraction in the 20-40 nm thick metal layer adjoining the metal-oxide interface, in which the metallic voids were located.[3] Figure 12 shows the same monotonically decreasing trends for S_d and the oxide void concentration, suggesting a linear relation between S_d and the oxide void concentration. Thus, the void concentration in the anodic oxide film is apparently controlled by, and scales with, the concentration of interfacial metallic voids prior to anodizing.

An explanation of the scaling of the oxide void concentration with S_d is that oxide voids form by incorporation of metallic voids. As noted, the thickness of the oxide void layer exceeds that of the void-containing metal layer before oxidation, implying that a portion of the oxide voids must have arisen from metallic voids created during anodizing. Within the precision of the void depth profiles, no difference in concentration can be detected between the oxide voids from pre-existing metal voids and those from metal voids formed during anodizing. Therefore, if it is accepted that oxide voids arise from metallic voids, the profiles support the inference that the surface concentration of metal voids formed by anodizing is the same as that of pre-existing metal voids. The same conclusion was drawn from the PAS study of anodic oxidation, from the invariance of S_d with oxide film thickness.[5] These observations support the interpretation that, as interfacial metal voids are incorporated into the oxide, new metal voids are generated at the same sites.

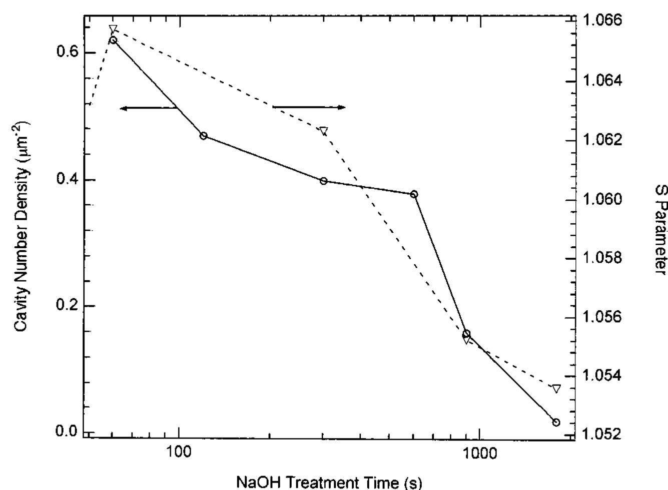

Figure 12. Mean void number density in inner portion of anodic films (left axis), plotted *vs.* NaOH treatment time. Anodizing voltage ranged from 53 to 106 V. Also shown on the right axis is the S parameter of positron annihilation radiation for NaOH-treated foils without anodic films.

These interfacial sites where voids are formed are determined in the present experiments by the NaOH treatment time. The AFM and TEM images obtained in this work suggest that void sites are associated with ridges on the surface topography. Although this correspondence may suggest an interface curvature-dependent mechanism for void formation, such ridge sites have also been associated with elevated concentrations of interfacial impurities.[15,23,24] Therefore, it cannot be said at this point whether void formation is induced by topographic or compositional inhomogeneities. The association of corrosion pits with these same ridge sites has been noted earlier, supporting the hypothesis that pits initiate at interfacial metallic voids.

Evidence for repeated formation of voids at topographic asperities during anodic oxidation of aluminum has been presented previously. Using TEM, Ono found strings of voids in anodic alumina films, extending perpendicular to the metal-oxide interface above ridges.[6,7] Macdonald later interpreted these experiments in terms of formation during oxidation and subsequent incorporation into the film of metallic voids.[25] In his interpretation, void formation was sensitive to the local interface curvature. Other interpretations of voids in amorphous anodic alumina films are based on concepts of oxygen gas evolution[7] or densification of the material around the void in the early stages of crystallization.[8] It is not clear how these mechanisms would be consistent with the relationship between oxide voids and metal voids, as demonstrated here. Also, as mentioned earlier, no diffraction was found in the oxide surrounding voids, as would be the case if voids formed due to localized crystallization.

If oxide voids are metallic voids incorporated into the film, it may be reasonable to assume that the metallic and oxide voids are roughly the same size. At least, no mechanism is known which would produce a large volume increase upon incorporation. The oxide voids detected in this work are equivalent in size to the order of 10^5-10^6 metal atoms, implying a surprisingly high growth rate at room temperature. Some speculation about the large void size can be mentioned. The transport of Al atoms away from the void, which determines its growth rate, can be viewed as the diffusion of metal atoms to the metal-oxide interface, followed by migration of metal ions in the oxide layer. The kinetics of both processes must be facile to account for the large void size. Therefore, it is suggested that metallic void formation occurs at special sites that permit rapid migration of metal atoms through the film, and also that the voids contact the metal-oxide interface at these sites. The latter characteristic would permit metal atoms to be removed by surface diffusion along the metal-void interface, as opposed to much slower volume diffusion through the metal. Dislocations near the interface can also provide high-diffusivity paths from any buried voids. Other factors such as localized atomic hydrogen absorption, which can significantly reduce the energy of aluminum vacancy formation, may also play a role in void growth.[26]

Conclusions

Microscopic observations of anodic aluminum oxide films with both TEM and AFM revealed the presence of voids tens of nanometers wide within the film. In the AFM measurements, depth profiles of voids in the film were obtained by imaging the film surface following partial dissolution of the oxide layer. The geometric characteristics of the voids revealed by both techniques were in quantitative agreement. Voids were distributed through the inner 60% of the film thickness, which indicated that they were formed at the metal-oxide interface during film growth. The number of voids scaled with the quantity of metallic interfacial voids present before anodizing, as detected by PAS. An explanation of this relationship is that oxide voids are metallic interfacial voids incorporated during anodizing. The uniform AFM depth profiles of oxide voids suggested that me-

Downloaded on 2014-09-11 to IP 129.186.176.188 address. Redistribution subject to ECS terms of use (see ecsdl.org/site/terms_use) unless CC License in place (see abstract).

tallic voids are created during anodic oxide growth, but that the concentration of these created voids is the same as that of the preexisting voids. The same conclusion was drawn from a PAS study of anodic oxidation,[4] and it supports a model in which new metallic voids are regenerated at the same sites formerly occupied by voids incorporated in the oxide layer. This regeneration of voids suggests that void formation is strongly favored at particular surface sites, rather than occurring at random locations on the surface.

Acknowledgments

Financial support for this work was provided by St. Jude Medical Corporation. Aluminum foils were donated by Nippon Chemi-Con.

Iowa State University assisted in meeting the publication costs of this article.

References

1. H. H. Strehblow, in *Corrosion Mechanisms in Theory and Practice*, 2nd ed., P. Marcus, Editor, p. 243, Dekker, New York (2002).
2. X. Wu, P. Asoka-Kumar, K. G. Lynn, and K. R. Hebert, *J. Electrochem. Soc.,* **141**, 3361 (1994).
3. K. R. Hebert, H. Wu, T. Gessmann, and K. G. Lynn, *J. Electrochem. Soc.,* **148**, B92 (2001).
4. H. Wu, K. R. Hebert, T. Gessmann, and K. G. Lynn, *J. Electrochem. Soc.,* **149**, B108 (2002).
5. C. E. Caicedo-Martinez, E. Koroleva, P. Skeldon, G. E. Thompson, G. Hoellrigl, P. Bailey, T. C. Q. Noakes, H. Habazaki, and K. Shimizu, *J. Electrochem. Soc.,* **149**, B139 (2002).
6. S. Ono, H. Ichonose, and N. Masuko, *J. Electrochem. Soc.,* **138**, 3705 (1991).
7. S. Ono, H. Ichonose, and N. Masuko, *J. Electrochem. Soc.,* **139**, L80 (1992).
8. R. S. Alwitt, C. K. Dyer, and B. Noble, *J. Electrochem. Soc.,* **129**, 711 (1982).
9. A. Despic and V. P. Parkhutik, in *Modern Aspects of Electrochemistry*, Vol. 20, J. O'M. Bockris, R. E. White, and B. E. Conway, Editors, p. 401, Plenum, New York (1989).
10. H. Takahashi, K. Fujimoto, H. Konno, and M. Nagayama, *J. Electrochem. Soc.,* **131**, 1856 (1984).
11. K. R. Hebert, T. Gessmann, P. Asoka-Kumar, and K. G. Lynn, *J. Electrochem. Soc.,* **151**, B22 (2004).
12. Z. Ashitaka, G. E. Thompson, P. Skeldon, G. C. Wood, and K. Shimizu, *J. Electrochem. Soc.,* **146**, 1380 (1999).
13. G. E. Thompson, P. E. Doherty, and G. C. Wood, *J. Electrochem. Soc.,* **129**, 1515 (1982).
14. C.-F. Lin and K. R. Hebert, *J. Electrochem. Soc.,* **137**, 3723 (1990).
15. T. Martin and K. R. Hebert, *J. Electrochem. Soc.,* **148**, B101 (2001).
16. Z. Ashitaka, G. E. Thompson, P. Skeldon, G. C. Wood, H. Habazaki, and K. Shimizu, *J. Electrochem. Soc.,* **147**, 132 (2000).
17. X. Wu and K. R. Hebert, *J. Electrochem. Soc.,* **143**, 83 (1996).
18. J. W. Diggle, T. C. Downie, and C. W. Goulding, *Chem. Rev. (Washington, D.C.),* **69**, 365 (1969).
19. J. Scherer, O. M. Magnussen, T. Ebel, and R. J. Behm, *Corros. Sci.,* **41**, 35 (1999).
20. A. Dekker and A. Middlehoek, *J. Electrochem. Soc.,* **117**, 440 (1970).
21. H. Takahashi and M. Nagayama, *Corros. Sci.,* **18**, 911 (1978).
22. F. Brown and W. D. Mackintosh, *J. Electrochem. Soc.,* **120**, 1096 (1973).
23. F. B. Cuff and N. J. Grant, *J. Inst. Met.,* **87**, 248 (1958-59).
24. C. E. Caicedo-Martinez, G. E. Thompson, and E. V. Koroleva, *Surf. Eng.,* **18**, 145 (2002).
25. D. D. Macdonald, *J. Electrochem. Soc.,* **140**, L27 (1993).
26. H. K. Birnbaum, C. Buckley, F. Zeides, E. Sirois, P. Rozenak, S. Spooner, and J. S. Lin, *J. Alloys Compd.,* **253-254**, 260 (1997).

Downloaded on 2014-09-11 to IP 129.186.176.188 address. Redistribution subject to ECS terms of use (see ecsdl.org/site/terms_use) unless CC License in place (see abstract).